NURETH14-362

NUMERICAL SIMULATIONS OF THE TOPFLOW-PTS STEAM-WATER EXPERIMENT

P. Apanasevich, D. Lucas and T. Höhne

Helmholtz-Zentrum Dresden-Rossendorf e.V., Institute of Safety Research P.O.Box 510119, 01314 Dresden, Germany P.Apanasevich@hzdr.de, D.Lucas@hzdr.de, T.Hoehne@hzdr.de

Abstract

The correct analysis of the Pressurized Thermal Shock requires the simulation of the thermal mixing that occurs when cold Emergency Core Cooling (ECC) water is injected into the cold leg, where it flows to the downcomer and mixes with the hot coolant present in the primary circuit. In the framework of the NURISP (Nuclear Reactor Integrated Simulation Project) project attempts are being made to improve the CFD modeling for two-phase PTS scenarios. For this purpose, two steady-state reference cases from the TOPFLOW-PTS experimental program were defined: one for air-water and one for steam-water flow. The current paper focuses only on the steamwater reference case. The pre-test simulations were performed with the commercial CFD code ANSYS CFX 12.0. The simulations of the steam-water reference test predicted a thermal stratification in the cold leg at the entrance into the downcomer and in the downcomer itself.

Introduction

Pressurized Thermal Shock (PTS) has been identified as one of the most important industrial needs related to nuclear reactor safety. It occurs when there are large thermal loads on the Reactor Pressure Vessel wall. The PTS analysis is required to assure the integrity of the Reactor Pressure Vessel (RPV) throughout the reactor life. Several scenarios that describe the phenomena in Small Break Loss Of Coolant Accidents result in an Emergency Core Cooling (ECC) water injection into the cold leg of a pressurized Water Reactor (PWR). The cold water in the cold leg mixes with the hot coolant, which is present in the primary circuit. The mixture flows to the downcomer where further mixing of the fluids takes place. In the case of two-phase PTS situations, the water level in the RPV has dropped down to or below the height of the cold leg nozzle, which leads to a partially filled or totally uncovered cold leg. In order to predict thermal gradients in the structural components of the Reactor Pressure Vessel wall, knowledge of transient temperature distribution in the downcomer is needed. For the prediction of the temperature distribution, reliable Computational Fluid Dynamic simulations are required. The CFD models should be able to model the complex mixing processes that take place in the cold leg and the downcomer of the reactor pressure vessel ([1], [2] and [3]).

Although, there are a number of experiments, where flow phenomena have been investigated via separate effects tests (see e.g. [4], [5], [6], [7], [8], [9] and [10]), there is still a need for well-instrumented experiments of combined phenomena for validation and demonstration purposes. There is also a requirement for experimental parameters to be varied in order to investigate key

PTS phenomena. High-resolution data are required in both space and time for the whole domain of interest. For this purpose, the TOPFLOW-PTS experimental program has been conceived [11]. Its objective is to provide a well-informed experimental database for both the validation of CFD modeling of the two-phase flow in the cold leg and downcomer and to improve the understanding of the thermal hydraulic phenomena involved. The experimental program consists of steady-state and transient tests that are performed with and without mass transfer due to condensation.

Currently available CFD codes are not able to simulate accurately all phenomena that occur in the cold leg and the downcomer during the ECC injection. Numerical simulations have already been performed with moderate success, e.g. [8], [12], [13], [14] and [15]. In order to improve the CFD modeling for two-phase PTS situations, two reference cases from the TOPFLOW-PTS experimental program were selected: one for steady air-water and one for steady steam-water flow.

The paper presents the pre-test simulations of TOPFLOW-PTS steam-water reference experiment by using CFD code ANSYS CFX 12.0. The experiment will be carried out on the TOPFLOW-PTS test facility of the Helmholtz-Zentrum Dresden-Rossendorf (HZDR). The effect of heat transfer between structures and fluid was not considered in the simulations.

1. Numerical simulations

1.1 Mathematical models

In the present numerical study, the Euler-Euler approach is used. General conservation equations for mass, momentum and energy can be respectively given as:

$$\frac{\partial(\alpha_k \rho_k)}{\partial t} + \nabla(\alpha_k \rho_k U_k) = \Gamma_k \tag{1}$$

$$\frac{\partial (\alpha_k \rho_k)}{\partial t} + \nabla (\alpha_k \rho_k U_k U_k) = -\alpha_k \nabla p_k + \alpha_k \rho_k g + \nabla \alpha_k (\tau_k + \tau_k^T) + M_k$$
(2)

$$\frac{\partial(\rho_{k}\alpha_{k}H_{k})}{\partial t} + \nabla \cdot (\rho_{k}\alpha_{k}U_{k}H_{k}) = \nabla \cdot (\alpha_{k}\lambda_{k}\nabla T) + \nabla \alpha_{k}(\tau_{k} + \tau^{T}_{k}) + F(H_{Sat,S} - H_{L}) + HTC_{L}A(T_{Sat,S} - T_{L})$$
(3)

where the k denotes liquid or gas phase, α is the volume fraction, ρ is the density, U is the velocity vector, p is the pressure, common for two phases, g is the gravitational acceleration, τ_k and τ_k^T are the average molecular shear stress and the turbulent shear stress, respectively, the vector M_k is the average interfacial momentum transfer between phases, H_k is the static enthalpy, Γ_k is the interphase mass source per unit volume, T is the temperature and HTC_L is the heat transfer coefficient for water. Both phases are assumed continuous and compressible.

[2], [3] reported that there are different flow morphologies during a PTS situation with a partially filled cold leg. Those are dispersed flow that occurs due to bubble entrainment, stratified flow

with a free surface and droplet flow. The bubble entrainment arises from the drag force. The drag force is most conveniently expressed in terms of the dimensionless drag coefficient C_D :

$$F_D = C_D A \rho_{Mix} \left| \left(U_L - U_G \right) \right|^2 \tag{4}$$

where ρ_{Mix} is the average density, A is the interfacial area density and $|(U_L - U_G)|^2$ is the relative (slip) velocity. In the simulations performed with the two-fluid model available in ANSYS CFX, the momentum exchange coefficients (interfacial area density and drag coefficient) are independent of the flow morphology:

$$A = |\nabla \alpha| \tag{5}$$

$$C_D = 0.44 \tag{6}$$

In order to improve the representation of the physics, separate models are necessary for dispersed and the separated continuous phases. For that reason, Egorov [12] proposed an Algebraic Interfacial Area Density (AIAD) model, where the momentum exchange coefficient depends on the local morphology. The basic conceptions of the AIAD model are:

- Detection of the morphological form of the flow and the corresponding switching for each correlation from one object pair to another
- The gas volume fraction is used as a criterion to differentiate between different flow regimes
- It provides a law for interfacial area density and the drag coefficient for full range $0 \le \alpha_G \le 1$
- The interfacial area density in the intermediate range is set to the interfacial area density for the free surface

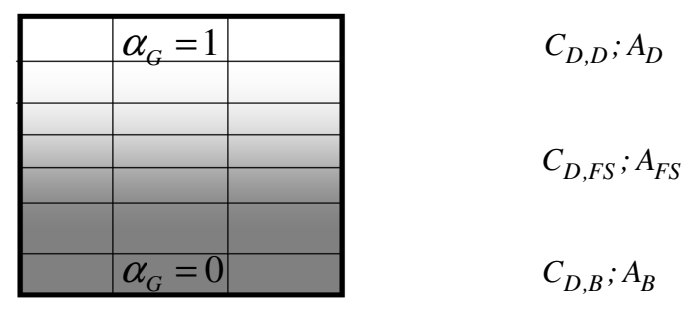


Figure 1: AIAD model: air volume fraction and corresponding flow morphologies

The interfacial area density also depends on the morphology of the phases. For bubbles and droplets, the interfacial area density is defined as follows

$$A_{B,D} = \frac{6\alpha_{G,L}}{d_{B,D}} \tag{7}$$

where $d_{B,D}$ is the bubble or droplet diameter and $\alpha_{G,L}$ is the gas or liquid volume fraction. For the free surface, the interfacial area density is defined as absolute value of the gas void fraction gradients:

$$A_{FS} = \left| \nabla \alpha_G \right| \tag{8}$$

The average density is defined as

$$\rho_{Mix} = \rho_G \alpha_G + \rho_L \alpha_L \tag{3/14}$$

(9)

where ρ_G and ρ_L are the gas and liquid densities, respectively. According to the flow regime, the corresponding interfacial area densities and drag coefficients are used. A simple switching procedure for the interfacial area density and drag coefficient uses a blending function f, which is defined for bubble and droplet regimes as follows

$$f_B = \frac{1}{1 + e^{A_B \left(\alpha_G - \alpha_{B,LIMIT}\right)}} \tag{10}$$

$$f_D = \frac{1}{1 + e^{A_D \left(\alpha_L - \alpha_{D,LIMIT}\right)}} \tag{11}$$

The blending function for the free surface is defined then as

$$f_{FS} = 1 - f_B - f_D \tag{12}$$

The area density and the drag coefficient in the whole domain can be defined as

$$A = f_B A_B + f_{FS} A_{FS} + f_D A_D \tag{13}$$

$$C_D = f_B C_{D,B} + f_{FS} C_{D,FS} + f_D C_{D,D}$$
 (14)

In the simulation of the steam-water reference test, void fraction limits of $\alpha_{D,LIMIT} = 0.3$ respectively $\alpha_{B,LIMIT} = 0.3$ and blending coefficients of $A_B = A_D = 800$ were used.

The next important consideration is how to model the free surface drag. Höhne [16] extended the AIAD model to determinate the drag coefficient of the free surface. It is reasonable to expect that the velocities of both fluids in the vicinity of the interface are rather similar.

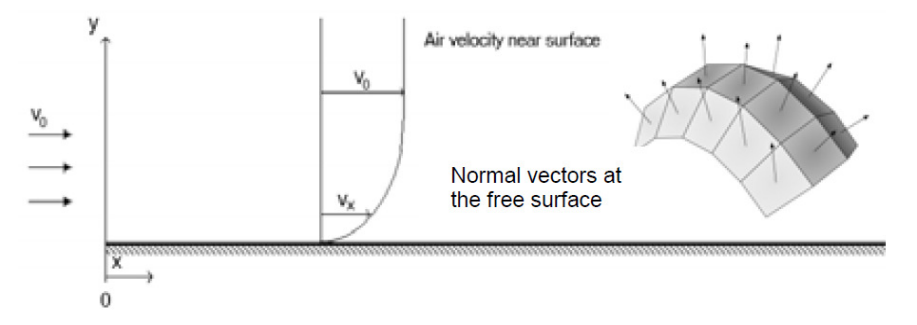


Figure 2: Air velocity near the free surface [16]

For that reason, a shear stress like a wall shear stress is assumed near the surface from both sides to reduce the velocity differences of both phases (cf. Fig 2). A viscous fluid moving along a "solid" like boundary will incur a shear stress. The morphology region "free surface" is considered as a boundary layer where the shear stress is imparted onto the boundary as a result of a loss of velocity $\frac{\partial u}{\partial v}$:

$$\tau_w = \mu \frac{\partial u}{\partial y} \bigg|_{y=0} \tag{15}$$

It is then assumed that the drag force is equal to the wall shear stress force acting at the free surface in the vicinity of the free surface:

$$F_w = \tau_i A = F_D \tag{16}$$

Substitution of equation (4) into equation (16) gives the free surface drag coefficient:

$$C_D = \frac{2\left[\alpha_G \tau_G + \alpha_L \tau_L\right]}{\rho_{Mix} U_{slip}^2} \tag{17}$$

where τ_G and τ_L are wall shear stresses of the gas and liquid phases, respectively. The wall shear stress of each fluid phase is calculated as follows

$$\tau_{L,G} = \mu_{L,G} \sqrt{\frac{\partial u_{x,L,G}}{\partial x} \cdot \frac{\partial \alpha_{L,G}}{\partial x}} + \left(\frac{\partial u_{y,L,G}}{\partial y} \cdot \frac{\partial \alpha_{L,G}}{\partial y}\right)^2 + \left(\frac{\partial u_{z,L,G}}{\partial z} \cdot \frac{\partial \alpha_{L,G}}{\partial z}\right)^2 + \left(\frac{\partial u_{z,L,G}}{\partial z} \cdot \frac{\partial \alpha_{L,G}}{\partial z}\right)^2}$$
(18)

where
$$\frac{\left(\frac{\partial \alpha_{L,G}}{\partial x}\right)}{A_{FS}}$$
, $\frac{\left(\frac{\partial \alpha_{L,G}}{\partial y}\right)}{A_{FS}}$ and $\frac{\left(\frac{\partial \alpha_{L,G}}{\partial z}\right)}{A_{FS}}$ are the components of the normal vector that are taken

from the gradients of the void fraction in x, y and z directions.

Finally, the modified drag coefficient of the free surface depends on the viscosity, the void fraction of both phases, the local gradients of gas and liquid velocities normal to the free surface and the slip velocity between the phases. The drag coefficient of the bubble and droplet morphologies assumes a constant value of 0.44 (Eq. 6).

Turbulence was modeled with Shear Stress Transport (SST) model. This model is a combination of k- ε and k- ω model and it is available with automatic wall functions. The choice of the turbulence model is taken on the basis of the personal experiences and the facts that this two-equation models offer a good compromise between complexity, accuracy and robustness [16]. Buoyancy was taken into account by the direction of gravity term.

Direct contact condensation (DCC) takes place in the ECC injection region and it also occurs at the free surfaces of the stratified flow. Heat transfer of direct contact condensation is characterized by the transport of heat and mass through a moving steam-water interface. The essential closure law for DCC is the heat transfer coefficient between the liquid and the interface. Several studies (see e.g. [7], [9], [18]) showed that condensation phenomena strongly depend on the turbulence in the liquid layer, where turbulent eddies transport the heat away from the interface. For this reason, we chose to use a heat transfer correlation, which is based on the surface renewal theory introduced by Hughes and Duffey ([13], [18]):

$$HTC_{L} = \frac{2}{\sqrt{\pi}} \rho_{L} c_{p,L} \sqrt{a_{L}} \sqrt[4]{\frac{\varepsilon}{\mu_{L} / \rho_{L}}}$$

$$\tag{19}$$

where ρ_L denotes liquid density, $c_{p,L}$ is liquid specific heat capacity at constant pressure, a_L is liquid thermal diffusivity, μ_L is liquid viscosity and ε is turbulence dissipation rate modeled with turbulence model.

A CFX built-in model called the two-resistance model has been chosen to define mass and heat transfers between the two phases. According to this model, the heat transfer processes on either side of the interface are considered separately by using two heat transfer coefficients, which are defined on each side of the interface. A zero resistance condition was set to specify heat transfer between the steam and the interface, i.e. the fluid specific heat transfer coefficient was assumed infinite. To describe the phase change induced by interphase heat transfer, the CFX thermal phase change model has been chosen [19].

1.2 Geometrical model and grid

The EDF CPY 900 MWe PWR was defined as the reference plant for the TOPFLOW-PTS test facility. The geometrical scale of the test facility is 1:2.5. The TOPFLOW-PTS test facility was designed in a way to simplify the configuration in order to allow better access for instrumentation and analysis of the results. According to the design of the test facility the pump simulator, the cold leg with the ECC line, as well as the downcomer simulator were included to the CFD model (Fig 3). The geometrical model was generated using the CAD software Autodesk Inventor 2009.

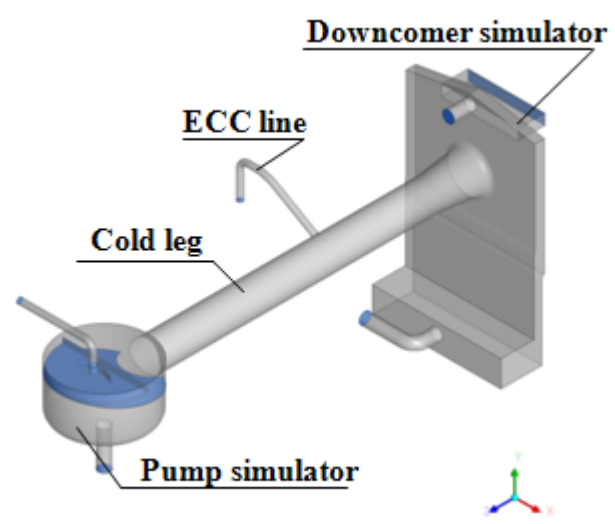


Figure 3: CFD model of the TOPFLOW-PTS test facility

ICEM CFD software [20] was used to generate the grid. Two hexahedral grids were generated for the geometry model. The base (coarse) grid consists of approximately 865,000 elements (Fig. 4a), and refined grid has approximately 1,670,000 elements (Fig. 4b). For the generation of the geometry and the grids best practice guidelines were considered as far as was reasonable.

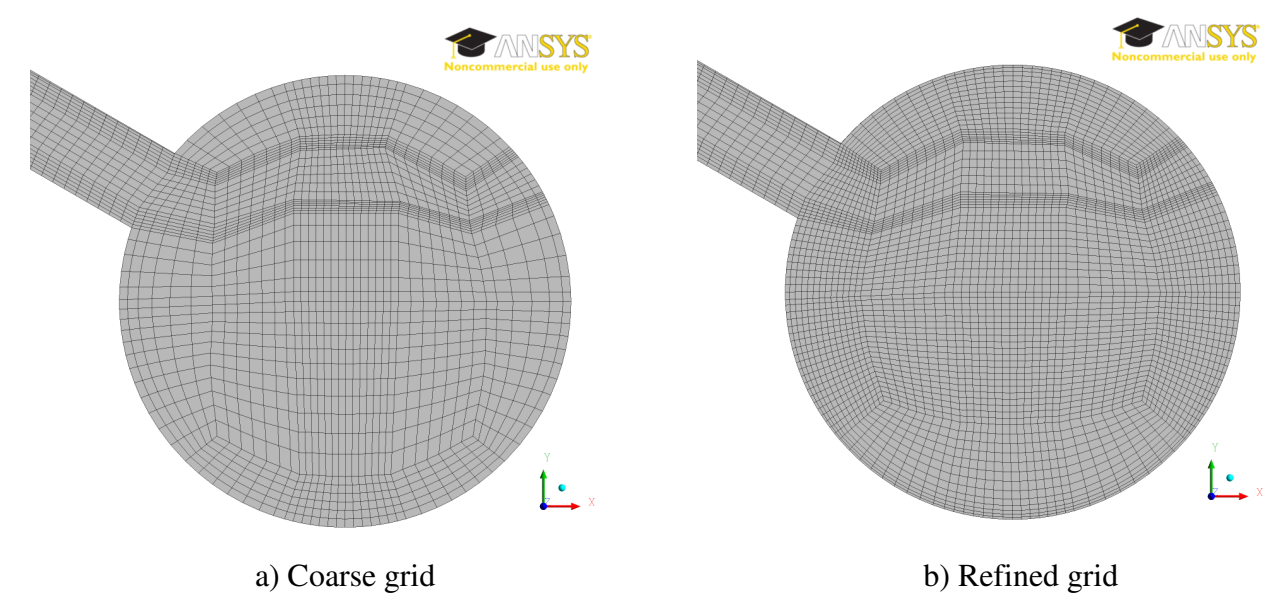


Figure 4: Numerical grids: coarse grid (a) and refined grid (b)

1.3 Boundary and initial conditions

The reference steam-water experiment will be carried out at a pressure of P_0 . The following boundary conditions were defined for the simulations. The cold leg was 50% full of water. The mass flow of ECC injection was MECC and the temperature of ECC water was TECC. The mass flow rate and temperature of pump simulator injection were MPS_in and TPS respectively. The relation of MPS_in to MECC was 1:1.7, while the liquid subcooling, TPS-TECC, amounted to 50K. The outlet flow rate of the pump simulator was MPS_out and it was equal to MPS_in. These operating conditions were defined in the experimental test matrix in order to avoid condensation in the pump simulator. To maintain steady-state conditions, the water level in the cold leg must be kept constant. For this reason, the downcomer outlet flow rate, MDC, was calculated as MECC + MCond (MCond = Total condensation rate). Saturated steam was supplied through a short pipe at the top of the front side of the downcomer. The steam in flow rate was Msteam. The steam surplus left the downcomer through the opening, which is connected to the condenser. On that boundary, the steam temperature was equal to the saturation temperature. The absolute values of the operating conditions are not given for a confidentiality agreement with the TOPFLOW-PTS consortium.

As an initial temperature, the saturation temperature was used. The pressure was initialized with the hydrostatic pressure. The fluid properties varied with pressure and temperature, where water tables provided by the International Association for the Properties of Water and Steam (IAPWS) were used.

The inlet boundaries were defined in the inlet leg to the pump simulator and in the ECC line. The outlet boundaries were set in the outflow pipes at the bottom of the pump simulator and the downcomer. The opening boundary was defined at the top of the reverse side of the downcomer. The boundary conditions given for the inlet boundaries were constant bulk mass flow rate, turbulence intensity (5%) and temperature. Bulk mass flow rate was set at both outlet boundaries. A constant opening pressure, opening temperature and turbulence intensity (1%) were specified at

the opening boundary. Due to the lack of the corresponding experimental data, the turbulence intensities at the inlet and opening boundaries were assumed on the basis of the personal experiences and the recommendations from the CFX User Manual.

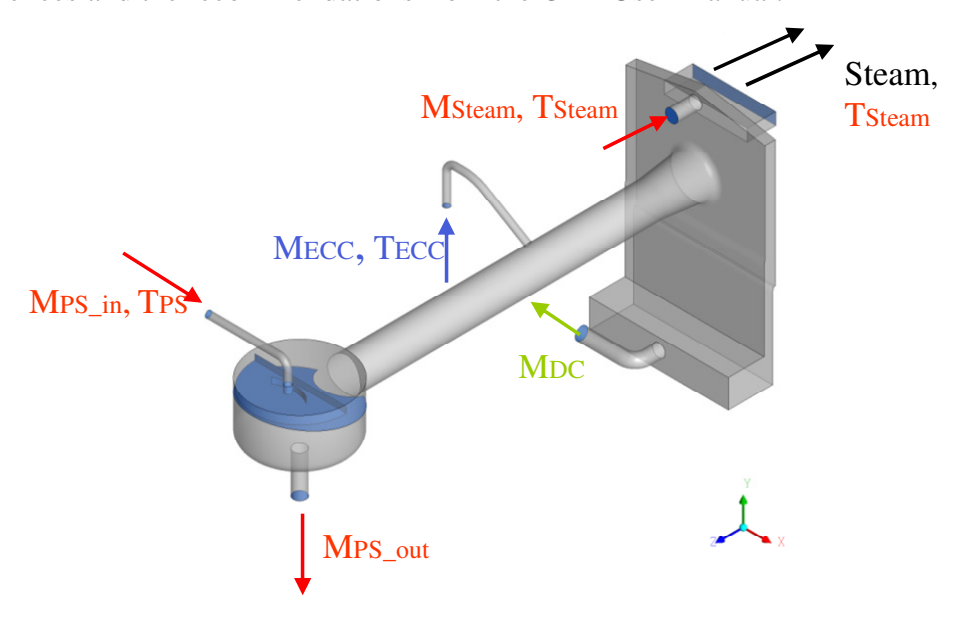


Figure 5: Boundary conditions for the steam-water case

1.4 Numerical scheme and nodalization

The coupled volume fraction algorithm has been chosen, as this option allows the implicit coupling of the discretized velocity, pressure and volume fraction equation in order to converge of calculations in fewer iteration loops. In the simulations shown below, the high-resolution discretization scheme was used to discretize the convective terms in the equations. A second order backward Euler scheme was used to approximate the transient terms. A root mean square (RMS) convergence criterion of 1×10^{-5} was used to ensure negligibly small iteration errors. Implementation of the AIAD model into CFX was done via the command language CCL. In the current study, the simulations were performed according to the BPGs described by Menter [17]. The simulations were performed on the HZDR LINUX cluster (Operating system: Linux Scientific 4.3 (64 bit), Node configuration: $2 \times AMD$ Opteron F 2220 (2.8 GHz, dual-core), 16 GB Memory). Four nodes (16 processors) were used for the transient simulations in a parallel mode with message passing protocol parallel virtual machine (PVM). The simulations took three months each to complete.

2. Results

In running the steam-water reference case, transient simulations were performed. A steady state was reached when RMS normalized values of the equation residuals became lower than $1x10^{-5}$ and the fluctuations of the main physical variables (temperature, velocity, pressure etc.) at different locations in the cold leg and the downcomer were negligible. The result obtained by using the

standard two-fluid model was used as an input for the simulation with the AIAD model in order to save computational time.

Eight locations were selected in the cold leg and the downcomer, which present the local temperature distribution. The locations correspond to the positions of the thermocouple lances used in the cold leg and the downcomer (Fig. 6). In the cold leg, the thermocouple lance LA1 is located upstream from the ECC injection point and the thermocouple lances LA2, LA4 and LA3 are located downstream from the ECC injection point. Thermocouple lances DCLA1, DCLA3, DCLA17 and DCLA20 are located in the downcomer.

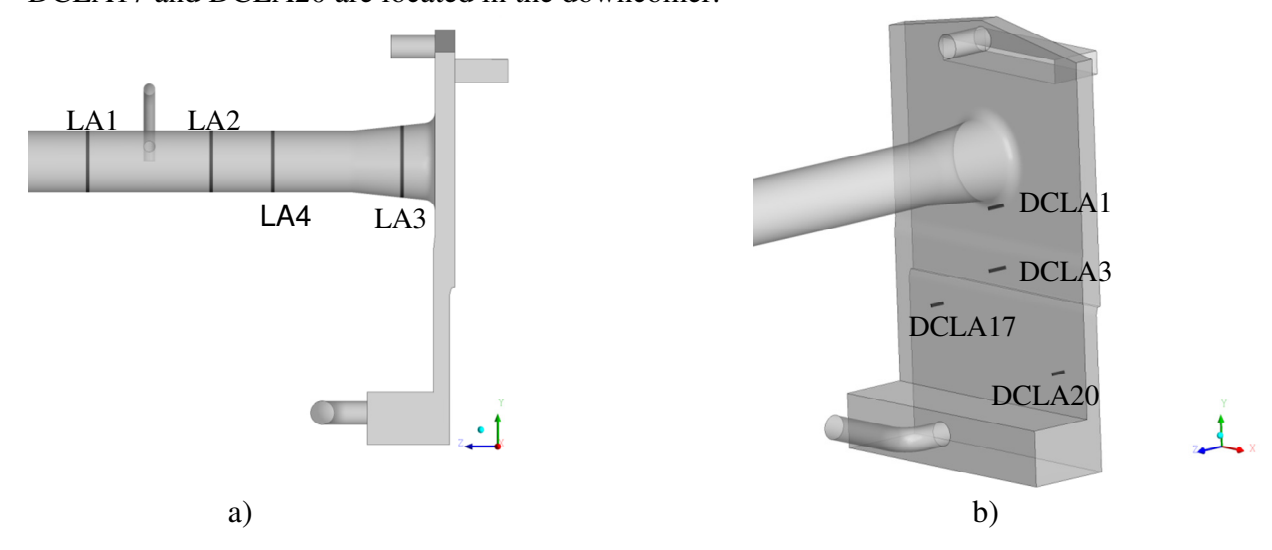


Figure 6: Locations of thermocouple lances in the cold leg (a) and the downcomer (b)

2.1 Cold leg

Figure 7 shows the temperature profiles in the cold leg that were calculated by using both the standard two-fluid model and the Algebraic Interfacial Area Density model. The red curve in Figure 7 represents the results obtained from the standard two-fluid model with constant fluid properties on the coarse grid, while the blue curve depicts the profile obtained for the standard two-fluid model with variable fluid properties on the coarse grid. The brown curve shows the result obtained by using the standard two-fluid model with variable fluid properties on the refined grid and the green curve shows the simulation obtained from the AIAD model with variable fluid properties on the refined grid. From the figure, it shown that depending on the definition of the fluid properties, we obtained different temperature profiles at the selected locations in the cold leg. The largest temperature difference is at the location of the thermocouple lance LA1, ECC upstream. The differences between simulations with constant and variable fluid properties can be explained through the use of constant fluid properties, where the full buoyancy effects are not taken into account. These effects can be considerable due to density difference between the fluids of different temperatures (cf. Fig. 8).

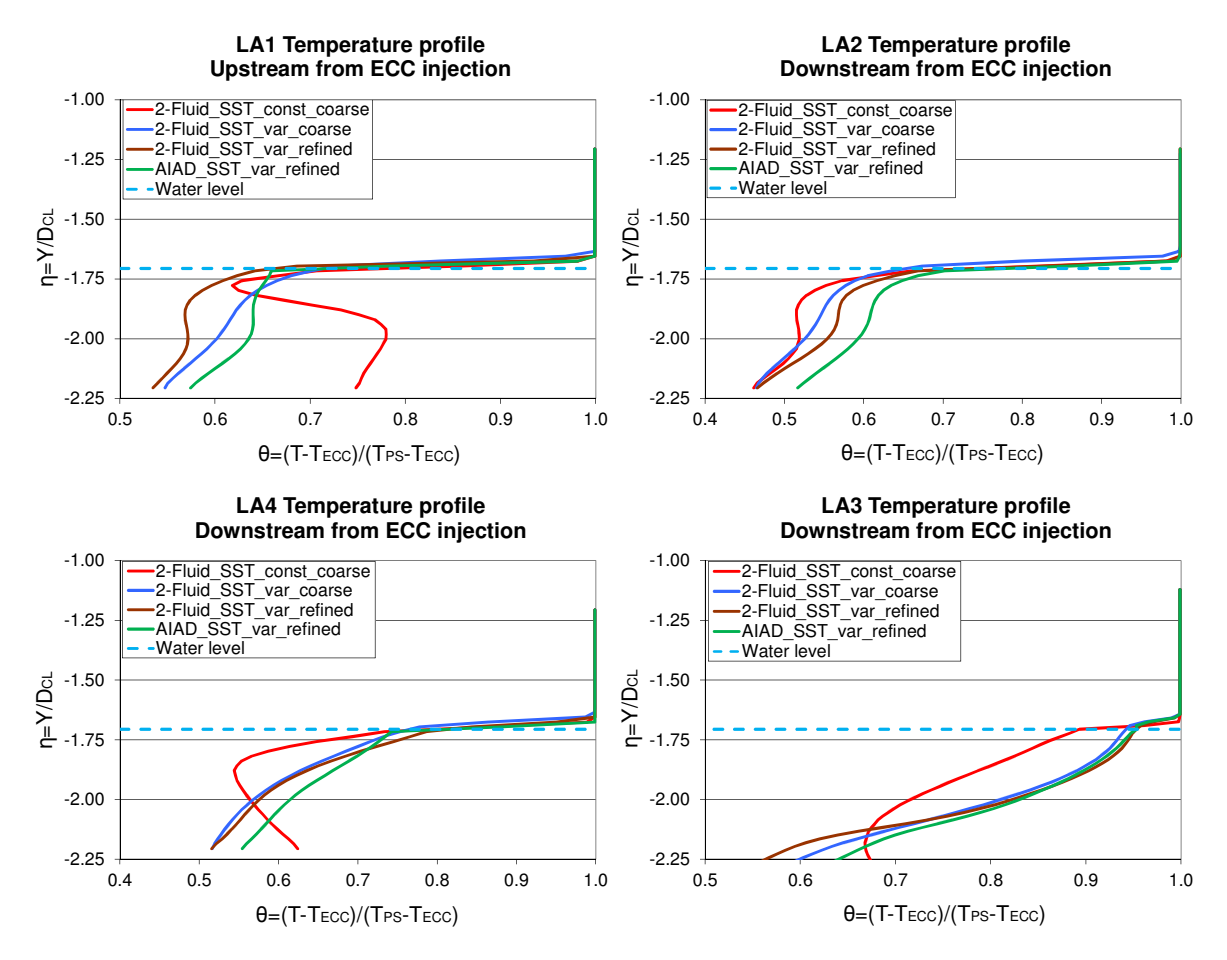


Figure 7: Temperature profiles in the cold leg

Two different grids were used to investigate the effect of the grid resolution. Comparison of the results indicates that the effect of the grid is considerable in the area close to the ECC jet injection at the locations of the thermocouple lances LA1 and LA2. At the locations of the LA3 and LA4, the effect of grid on the target variable (temperature) is negligible.

In comparison between the simulations with standard two-fluid model and the AIAD model on the refined grid, it is noticed that both models provided quite different results. Differences can be explained as follows. The standard two-fluid model and the AIAD model predicted the way the jet splits differently and how the resultant formations of the recirculation flow in the ECC upstream region were generated. In addition, both models predicted different condensation rates. The total condensation rate is 0.173kg/s when using the AIAD model, while they are 0.154kg/s and 0.164kg/s in case of use of the standard two-fluid model on the refined and coarse grids, respectively. These values of the total condensation rate were obtained in what was considered to have been a steady-state condition.

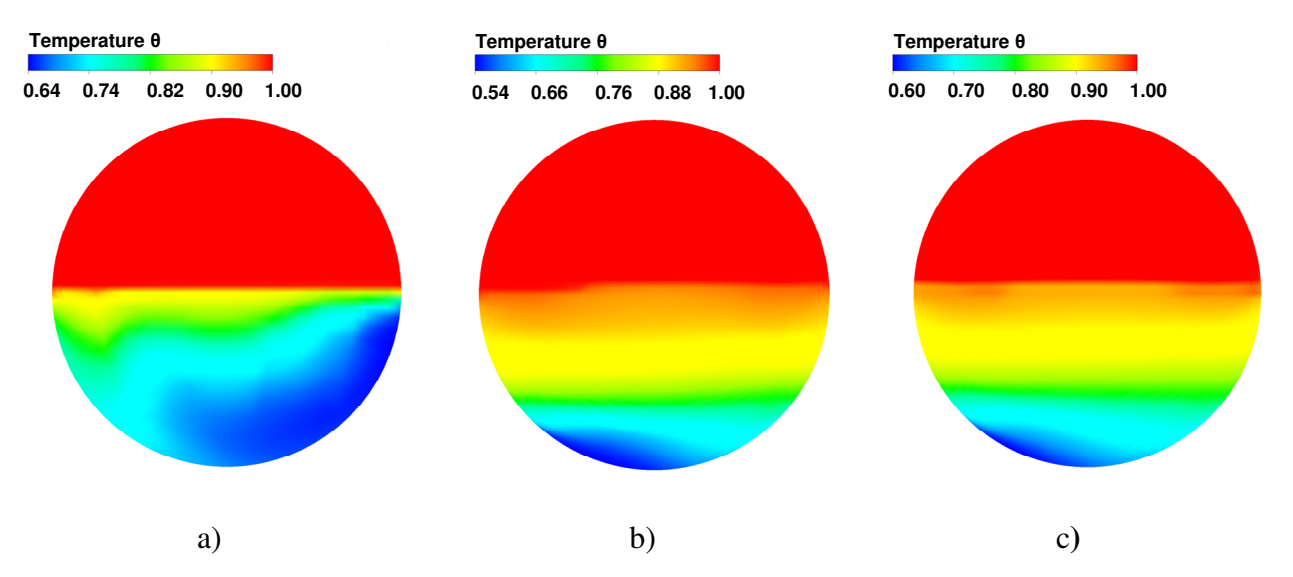


Figure 8: Temperature distribution in the whole cross-section of the cold leg at the entrance into the downcomer: a) standard two-fluid model with constant fluid properties (coarse grid), b) standard two-fluid with variable fluid properties (refined grid) and c) AIAD model with variable fluid properties (refined grid)

Finally, the temperature distribution in the whole cross section of the cold leg at the entrance into the downcomer is shown in Figure 8. The location of the plane corresponds to the location of the thermocouple lance LA3. In case of use of variable fluid properties, we can clearly observe a thermal stratification in the cold leg at the entrance into the downcomer.

2.2 Downcomer

Temperature profiles at the selected locations in the downcomer obtained by using the standard two-fluid model and the AIAD model are presented on Figure 9. The points with ζ = -0.035 and 0.05 are found on the downcomer reverse wall. Based on the temperature profiles at DCLA1, DCLA3, DCLA17 and DCLA20, it can be observed again that depending on the definition of the fluid properties and using different models (standard two-fluid model vs. AIAD model) different results were obtained. The main reason for it is that different models predicted different formations of the cold-water plume in the downcomer (cf. Fig. 10). In Figure 10 we see a clearly separated, meandering plumes, which differ in the width and propagation direction.

An accurate prediction of formation or lack of formation of the cold-water plume is essential for the further structural analyses and in general for the assessment of the safety aspects. Such a plume being in contact with the RPV wall for a long time cools it down. Since the cold-water plume has a relatively low temperature compared to the surrounding liquid, large thermal loads can occur on the RPV wall. Temperature difference, observed in the simulation in the region of the plume, need to be validated against the experimental data that will be obtained from the equivalent experiments.

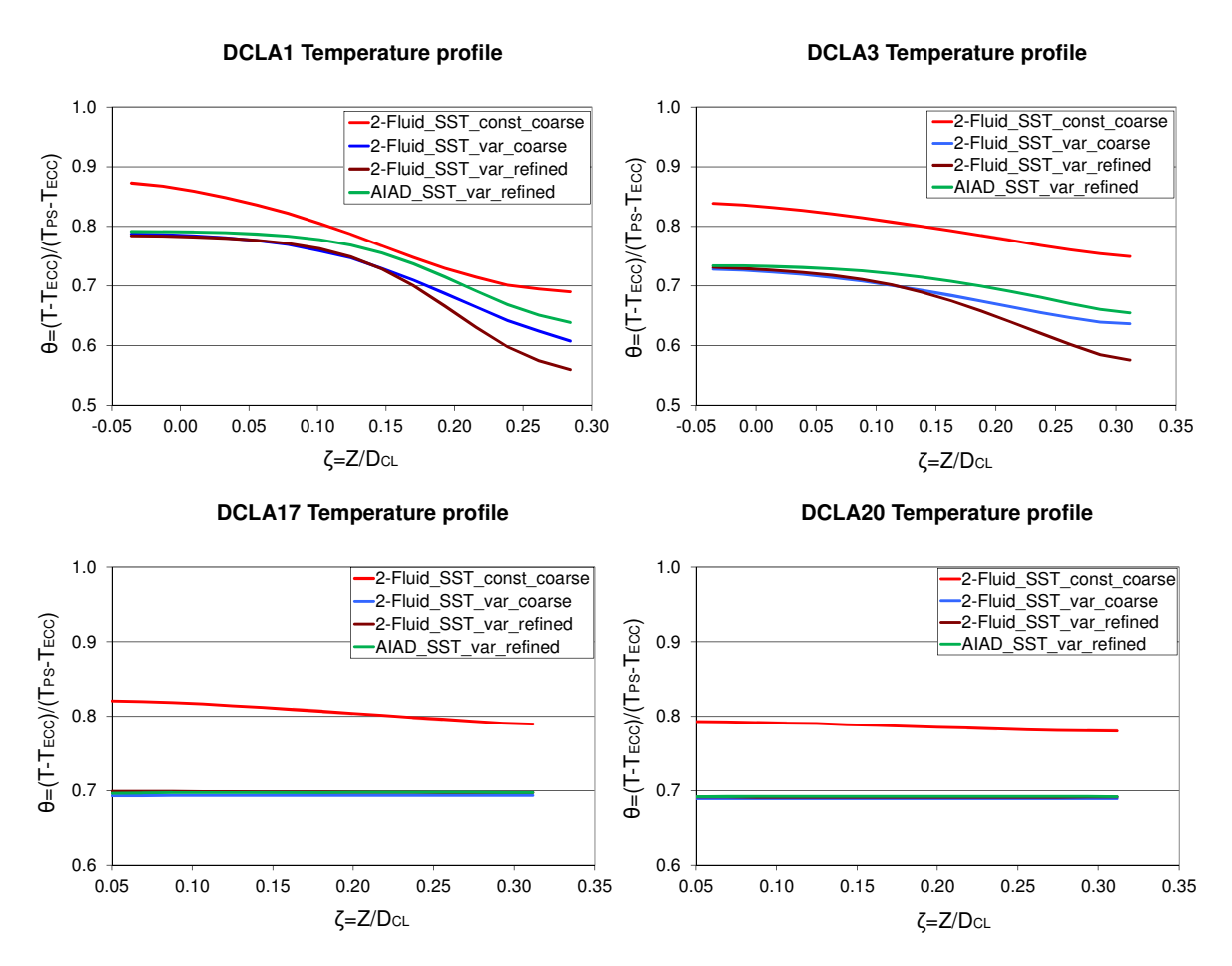


Figure 9: Temperature profiles in the downcomer

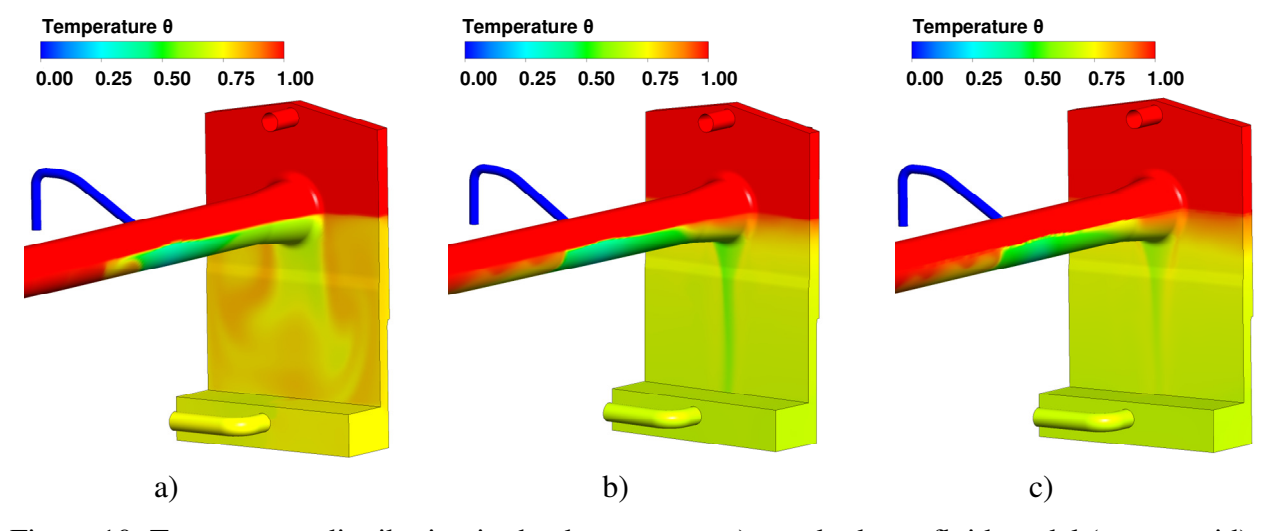


Figure 10: Temperature distribution in the downcomer: a) standard two-fluid model (coarse grid), b) standard two-fluid model (refined grid) and c) AIAD-model (refined grid)

3. Conclusions

Three-dimensional CFD simulations of the TOPFLOW-PTS steady-state steam-water experiment (with mass transfer between the phases) have been performed using the standard two-fluid model available in ANSYS CFX and the Algebraic Interfacial Area Density model. Direct contact condensation that takes place in both the cold leg and the downcomer was modeled using the surface renewal theory as written by Hughes and Duffey. Thermal stratification was predicted in the cold leg and in the downcomer. The total condensation rate in the simulation with the Algebraic Interfacial Area Density model was higher than in the simulation with the standard two-fluid model. The studies also showed that buoyancy effects are considerable due to the large temperature gradient calculated in the cold leg. In future work, the TOPFLOW-PTS experimental data will be used for the validation of the simulations described in this paper.

4. Acknowledgments

The work is financially supported by the NURISP (Nuclear Reactor Integrated Simulation Project) project. The NURISP project is partly funded by the European Commission in the framework of the Seventh Framework Program EURATOM (2009-2011). The TOPFLOW-PTS Experiments Project is financially supported by CEA, EDF, IRSN, AREVA (France); PSI, ETHZ (Switzerland); HZDR (Germany).

5. References

- [1] IAEA, "Guidelines on pressurized thermal shock analysis for WWER nuclear power plants. IAEA Document IAEA-EBP-WWER-08", (2001)
- [2] Lucas, D.; Bestion, D.; Bodèle, E.; Coste, P.; Scheuerer, M.; D'Auria, F.; Mazzini, D.; Smith, B.; Tiselj, I.; Martin, A.; Lakehal, D.; Seynhaeve, J.-M.; Kyrki-Rajamäki, R.; Ilvonen, M.; Macek, J., "An Overview of the Pressurized Thermal Shock Issue in the Context of the NURESIM Project", *Science and Technology of Nuclear Installations*, Volume 2009, Article ID 583259, 2009
- [3] Lucas, D.; Bestion, D.; Coste, P.; Pouvreau, J.; Morel, Ch.; Martin, A.; Boucker, M.; Bodele, E.; Schmidtke, M.; Scheuerer, M.; Smith, B.; Dhotre, M. T.; Niceno, B.; Lakehal, D.; Galassi, M. C.; Mazzini, D.; D'Auria, F.; Bartosiewicz, Y.; Seynhaeve, J.-M.; Tiselj, I.; ŠTrubelj, L.; Ilvonen, M.; Kyrki-Rajamäki, R.; Tanskanen, V.; Laine, M.; Puustinen, J., "Main results of the European project NURESIM on the CFD-modelling of two-phase Pressurized Thermal Shock (PTS)", Kerntechnik, 74(2009), pp. 238-242, 2009
- [4] Bonnetto, F., Lahey Jr., R.T., "An experimental study on air carry-under due to a plunging liquid jet", *International Journal of Multiphase Flow*, 19, pp. 281-294, (1993)
- [5] Fabre, J., Masbernat, L., Suzanne, C., "Stratified flow, Part I: local structures", *Multiphase Science and Technology*, 3, Ed. by G. F. Hewitt, J.M. Delhaye, and N. Zuber, pp. 285-301, (1987)
- [6] Iguchi, M., Okita, K., Yamamoto, F., "Mean velocity and turbulence characteristics of water flow in the bubble dispersion region induced by plunging water jet", *Int. J. Multi-phase Flow*, 24, pp. 523-537, (1998)

- [7] Lim, I. S., Tankin, R. S., Yuen, M. C., "Condensation measurement of horizontal cocurrent steam-water flow", *Journal of Heat Transfer*, 106, pp. 425-432, (1984)
- [8] Vallée, C., Höhne, T., Prasser, H.-M., Sühnel, T., "Experimental investigation and CFD simulation of air/water flow in a horizontal channel", <u>The 11th International Topical Meeting on Nuclear Reactor Thermal-Hydraulics (NURETH-11)</u>, Avignon, France, (2005)
- [9] Ruile, H., "Direktkondensation in geschichteten Zweiphasenströmungen", VDI-Fortschrittsbericht Reihe 19, Nr. 88, VDI-Verlag, Düsseldorf, (1996)
- [10] Puustinen, M., "Combined Effects Experiments with the Condensation Pool Experiments", Final Report, VTT Research Notes 2363, ISBN 951-38-6886-9, ISSN 1235-0605 (VTT 2006)
- [11] Peturaud, P., Hampel, U., Barbier, A., Dreier, J., Dubois, F., Hervieu, E., Martin, A. and Prasser, H.-M., "General overview of the TOPFLOW-PTS experimental program", <u>The 14th International Topical Meeting on Nuclear reactor Thermal Hydraulics (NURETH-14)</u>, Toronto, Ontario, Canada, September 25-29, (2011)
- [12] Egorov, Y., "Validation of CFD codes with PTS-relevant test cases", 5th Euratom Framework Programme ECORA project, (2004)
- [13] Štrubelj, L., Tiselj, I., "Numerical modelling of condensation of saturated steam on sub-cooled water surface in horizontally stratified flow", <u>The 12th International Topical Meeting on Nuclear Reactor Thermal Hydraulics (NURETH-12)</u>, Sheraton Station Square, Pittsburgh, Pennsylvania, U.S.A. September 30-October 4, (2007)
- [14] Coste, P., Laviéville, J., Pouvreau, J., Boucker, M., "A two-phase CFD approach to the PTS problem evaluated on COSI experiment", <u>Proc. The 16th International Conference on Nuclear Engineering ICONE16</u>, Orlando, Florida, USA, May 11-15, (2008)
- [15] Tiselj, I., Štrubelj, L., Prošek, A., "Direct contact condensation in horizontally stratified flow of AEKI PMK-2 device", 6th Euratom Framework Program NURESIM, Deliverable D2.1.13.1, (2006)
- [16] Höhne, T. and Vallée, C., "Numerical Prediction of Horizontal Two Phase Flow using an Interfacial Area Density Model", <u>Proc. The 13th International Topical Meeting on Nuclear Reactor Thermal Hydraulics (NURETH-13)</u>, Kanazawa, Japan (2009)
- [17] Menter, F., "CFD Best Practice Guidelines for CFD Code Validation for Reactor Safety Applications", ECORA FIKS-CT-2001-00154
- [18] Hughes, E. D., Duffey, R. B., "Direct contact condensation and momentum transfer in turbulent separated flows", *Int. J. Multiphase Flow*, 17, pp. 599-619, (1991)
- [19] ANSYS CFX-12.0 User Manual, 2009, ANSYS
- [20] ANSYS ICEM CFD-12.1 User Manuel, 2009, ANSYS